5578 *Chem. Mater.* **2009,** *21,* 5578–5584
DOI:10.1021/cm9020673

CHEMISTRY OF MATERIALS
Article

Metal Nanoparticle−Block Copolymer Composite Assembly and Disassembly

Zihui Li,[†,‡] Hiroaki Sai,[†,§] Scott C. Warren,[‡] Marleen Kamperman,[§] Hitesh Arora,[○] Sol M. Gruner,[#,▽] and Ulrich Wiesner*[,§]

[‡]*Department of Chemistry and Chemical Biology,* [§]*Department of Materials Science and Engineering,* [○]*School of Chemical and Bimolecular Engineering,* [#]*Department of Physics,* [▽]*Cornell High Energy Synchrotron Source (CHESS), and Cornell University, Ithaca, New York 14853.* [†]*These authors contributed equally to this work*

Received July 8, 2009. Revised Manuscript Received October 13, 2009

Ligand-stabilized platinum nanoparticles (Pt NPs) were self-assembled with poly(isoprene-*block*-dimethylaminoethyl methacrylate) (PI-*b*-PDMAEMA) block copolymers to generate organic−inorganic hybrid materials. High loadings of NPs in hybrids were achieved through usage of *N,N*-di-(2-(allyloxy)ethyl)-*N*-3-mercaptopropyl-*N*-methylammonium chloride as the ligand, which provided high solubility of NPs in various solvents as well as high affinity to PDMAEMA. From NP synthesis, existence of subnanometer Pt NPs was confirmed by high-angle annular dark field scanning transmission electron microscopy (HAADF-STEM) images. Estimations of the Pt NP ligand headgroup density based on HAADF-STEM images and thermogravimetric analysis (TGA) data yielded results comparable to what has been found for alkanethiol self-assembled monolayers (SAMs) on flat Pt {111} surfaces. Changing the volume fraction of Pt NPs in block copolymer−NP composites yielded hybrids with spherical micellar, wormlike micellar, lamellar, and inverse hexagonal morphologies. Disassembly of hybrids with spherical, wormlike micellar, and lamellar morphologies generated isolated metal NP−based nanospheres, cylinders, and sheets, respectively. Results suggest the existence of powerful design criteria for the formation of metal-based nanostructures from designer blocked macromolecules.

Introduction

Block copolymer (BCP) self-assembly is considered a powerful route to achieve nanoscale (2−50 nm) materials because of its ability to form various periodic structures with tunable length scale.[1−3] BCPs have been used as structure directing agents to incorporate different loadings of functional inorganic species into select blocks of BCPs, resulting in ordered nanostructured organic−inorganic hybrid materials.[4−6] BCPs in hybrids with high inorganic loading can be removed by chemical, photochemical, and/or thermal treatments without collapse of the structures, resulting in nanoporous functional materials. This methodology has been successfully applied to various inorganic systems, such as aluminosilicates,[7] orthosilicates,[8−10] transition metal oxides[11,12] and non-oxide ceramics.[13,14] Despite the achievements in the field, synthesizing ordered nanostructured metal hybrids and metals thereof using BCPs remains challenging due to the high surface energies of metals. To date, mainly two approaches are being utilized: the first involves in situ metal nanoparticles (NP) synthesis, where BCPs are loaded or swollen by metal precursors prior or after microphase separation, and a subsequent reducing step is applied to transform the metal precursors into metal NPs.[15−19] Different metals (e.g., Au, Pt, Pd, Ag) and

*To whom correspondence should be addressed. E-mail address: ubw1@cornell.edu.

(1) Bates, F. S. *Science* **1991**, *251*, 898.
(2) Bates, F. S.; Fredrickson, G. H. *Annu. Rev. Phys. Chem.* **1990**, *41*, 525.
(3) Cho, B.-K.; Jain, A.; Gruner, S. M.; Wiesner, U. *Science* **2004**, *305*, 1598.
(4) Kamperman, M.; Wiesner, U. *Block Copolymers in Nanoscience*; Lazzari, M.; Liu, G.; Lecommandoux, S., Eds.; WILEY-VCH Verlag GmbH & KgaA: Weinheim, 2006; p 309.
(5) Templin, M.; Franck, A.; DuChesne, A.; Leist, H.; Zhang, Y. M.; Ulrich, R.; Schadler, V.; Wiesner, U. *Science* **1997**, *278*, 1795.
(6) Hamdoun, B.; Ausserré, D.; Joly, S.; Gallot, Y.; Cabuil, V.; Clinard, C. *J. Phys. II France* **1996**, *6*, 493.
(7) Simon, P. F. W.; Ulrich, R.; Spiess, H. W.; Wiesner, U. *Chem. Mater.* **2001**, *13*, 3464.
(8) Bagshaw, S. A.; Prouzet, E.; Pinnavaia, T. J. *Science* **1995**, *269*, 1242.
(9) Tanev, P. T.; Pinnavaia, T. J. *Science* **1995**, *267*, 865.
(10) Zhao, D. Y.; Feng, J. L.; Huo, Q. S.; Melosh, N.; Fredrickson, G. H.; Chmelka, B. F.; Stucky, G. D. *Science* **1998**, *279*, 548.
(11) Yang, P. D.; Zhao, D. Y.; Margolese, D. I.; Chmelka, B. F.; Stucky, G. D. *Nature* **1998**, *396*, 152.
(12) Lee, J.; Orilall, M. C.; Warren, S. C.; Kamperman, M.; Disalvo, F. J.; Wiesner, U. *Nat. Mater.* **2008**, *7*, 222.
(13) Kamperman, M.; Garcia, C. B. W.; Du, P.; Ow, H. S.; Wiesner, U. *J. Am. Chem. Soc.* **2004**, *126*, 14708–14709.
(14) Wan, J. L.; Alizadeh, A.; Taylor, S. T.; Malenfant, P. R. L.; Manoharan, M.; Loureiro, S. M. *Chem. Mater.* **2005**, *17*, 5613.
(15) Chan, Y. N. C.; Craig, G. S. W.; Schrock, R. R.; Cohen, R. E. *Chem. Mater.* **1992**, *4*, 885.
(16) Chan, Y. N. C.; Schrock, R. R.; Cohen, R. E. *Chem. Mater.* **1992**, *4*, 24.
(17) Sankaran, V.; Cummins, C. C.; Schrock, R. R.; Cohen, R. E.; Silbey, R. J. *J. Am. Chem. Soc.* **1990**, *112*, 6858–6859.
(18) Spatz, J. P.; Herzog, T.; Mossmer, S.; Ziemann, P.; Moller, M. *Adv. Mater.* **1999**, *11*, 149.
(19) Yamauchi, Y.; Sugiyama, A.; Morimoto, R.; Takai, A.; Kuroda, K. *Angew. Chem., Int. Ed.* **2008**, *47*, 5371.

Published on Web 11/06/2009

polymers (e.g., poly(styrene-*block*-acrylic acid) (PS-*b*-PAA), poly(styrene-*block*-2-vinylpyridine) (PS-*b*-P2VP)) have been used, proving the generality of this approach. Although in situ methods are suitable for thin film applications, loading of the metals is limited by the diffusion of the reagents when applied to bulk materials with larger thickness. The second approach involves ex situ metal NP synthesis. Preformed metal NPs are self-assembled with block copolymers where the NPs are stabilized with tailored surface ligands or functional groups which render them compatible with only one block of the block copolymer.[20−26] Extensive studies of this method have been performed in the last nearly two decades both in thin films and in the bulk. For example, Au NPs stabilized with alkanethiol groups localized at the interface between a symmetric poly(styrene-*block*-ethylene-*co*-propylene) (PS-*b*-PEP) have been reported by Bockstaller et al.[20] Kim et al. studied PS-coated Au NPs self-assembled with PS-*b*-P2VP. They found that the addition of NPs increased the effective volume fraction of the PS block and thus induced a lamellar-to-cylindrical phase transition.[21] They also studied the effect of ligand headgroup density on NPs/polymer interaction.[22,23] Finally, more recently some of us reported the assembly of metal NPs in block copolymer brushes in which NP-BCP interactions are tuned, likewise, by ligand head density.[26]

Most of the work on BCP/metal NP self-assembly has focused on the dilute nanoparticle regime, where the NPs only comprise a small volume fraction of the hybrid material. Achieving hybrid synthesis in the dense nanoparticle regime[27] where NPs comprise the majority volume fraction will provide access to nanostructured organic−metal hybrid materials, as well as to nanoporous metals.[19,28,29] It has been reported in several BCP/NP systems that when the volume fraction of NPs increases, controlled microphase separation of the BCP was disrupted.[30,31] The observed macrophase separation could arise from poor particle solubility in solvents at high concentration, insufficient favorable enthalpic interactions between NPs and BCP as well as unfavorable entropic interactions.[32−34] Moreover, the small volume fraction of the core metal embedded in the corona when using polymer coated NPs leads to small metal loadings in the final material. Thus, in order to achieve BCP/metal NP hybrids with high metal loadings, the metal NPs have to be tailored to fulfill several criteria:[35,36]

1. NPs should maintain high solubility in polymer-compatible solvents.
2. There should be sufficient preferential interaction of NPs with one block of the BCP.
3. NP size should be smaller than the radius of gyration of the preferential block.
4. The ligand should be short enough to ensure a reasonable core/corona volume ratio.

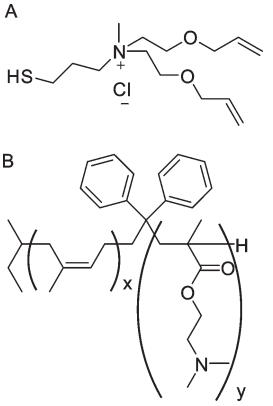

Figure 1. (A) *N*,*N*-di-(2-(allyloxy)ethyl)-*N*-3-mercaptopropyl-*N*-methyl-ammonium chloride, which is used as a ligand to stabilize Pt NPs. (B) Poly(isoprene-*block*-dimethylaminoethyl methacrylate) (PI-*b*-PDMAEMA) block copolymer.

Fulfilling these criteria, our group recently developed novel ligand-stabilized platinum NPs which self-assembled with poly(isoprene-*block*-dimethylaminoethyl methacrylate) (PI-*b*-PDMAEMA), see Figure 1.[35−37] The use of thiol-containing quaternary ammonium salts with ether chain ends as a ligand ensured Pt NPs' high solubility in polar solvents as well as dipole−dipole interactions with PDMAEMA. Aging of Pt NPs removed a small proportion of the ligands on the surface and greatly enhanced the morphology control in the structure formation process, possibly due to the chemisorption of amine groups that exist on each DMAEMA monomer unit to the metal surface. Inverse hexagonal and lamellar hybrid structures were obtained through this method. The ligand density on the NP surface was estimated based on average particle size as obtained from bright field transmission electron microscopy (BF-TEM) images and thermogravimetric analysis (TGA) results. In the

(20) Bockstaller, M. R.; Lapetnikov, Y.; Margel, S.; Thomas, E. L. *J. Am. Chem. Soc.* **2003**, *125*, 5276.
(21) Kim, B. J.; Chiu, J. J.; Yi, G. R.; Pine, D. J.; Kramer, E. J. *Adv. Mater.* **2005**, *17*, 2618.
(22) Kim, B. J.; Bang, J.; Hawker, C. J.; Kramer, E. J. *Macromolecules* **2006**, *39*, 4108.
(23) Kim, B. J.; Fredrickson, G. H.; Kramer, E. J. *Macromolecules* **2008**, *41*, 436–447.
(24) Chiu, J. J.; Kim, B. J.; Kramer, E. J.; Pine, D. J. *J. Am. Chem. Soc.* **2005**, *127*, 5036.
(25) Lin, Y.; Boker, A.; He, J. B.; Sill, K.; Xiang, H. Q.; Abetz, C.; Li, X. F.; Wang, J.; Emrick, T.; Long, S.; Wang, Q.; Balazs, A.; Russell, T. P. *Nature* **2005**, *434*, 55.
(26) Oren, R.; Liang, Z.; Barnard, J. S.; Warren, S. C.; Wiesner, U.; Huck, W. T. S. *J. Am. Chem. Soc.* **2009**, *131*, 1670.
(27) Jain, A.; Wiesner, U. *Macromolecules* **2004**, *37*, 5665.
(28) Attard, G. S.; Göltner, C. G.; Corker, J. M.; Henke, S.; Templer, R. H. *Angew. Chem., Int. Ed.* **1997**, *36*, 1315.
(29) Yamauchi, Y.; Yokoshima, T.; Mukaibo, H.; Tezuka, M.; Shigeno, T.; Momma, T.; Osaka, T.; Kuroda, K. *Chem. Lett.* **2004**, *33*, 542.
(30) Lo, C. T.; Lee, B.; Pol, V. G.; Rago, N. L. D.; Seifert, S.; Winans, R. E.; Thiyagarajan, P. *Macromolecules* **2007**, *40*, 8302.
(31) Park, J. H.; Sun, Y. J.; Goldman, Y. E.; Composto, R. J. *Macromolecules* **2009**, *42*, 1017.
(32) Huh, J.; Ginzburg, V. V.; Balazs, A. C. *Macromolecules* **2000**, *33*, 8085.
(33) Thompson, R. B.; Ginzburg, V. V.; Matsen, M. W.; Balazs, A. C. *Science* **2001**, *292*, 2469.
(34) Warren, S. C.; DiSalvo, F. J.; Wiesner, U. *Nat. Mater.* **2007**, *7*, 156.
(35) Warren, S. C.; Messina, L. C.; Slaughter, L. S.; Kamperman, M.; Zhou, Q.; Gruner, S. M.; DiSalvo, F. J.; Wiesner, U. *Science* **2008**, *320*, 1748.
(36) Warren, S. C.; Wiesner, U. *Pure Appl. Chem.* **2009**, *81*, 73.
(37) Warren, S. C.; Banholzer, M. J.; Slaughter, L. S.; Giannelis, E. P.; DiSalvo, F. J.; Wiesner, U. *J. Am. Chem. Soc.* **2006**, *128*, 12074.

present paper, a full account of these results is given. First, we revisit the question of the ligand density on the Pt NPs. Then, we explore the morphology space of PI-*b*-PDMAEMA/Pt NP hybrids, revealing the accessibility of two new morphologies by varying Pt NP/PI-*b*-PDMAEMA ratios. Finally, we discuss the preparation of shape controlled metal nano-objects by disassembly of Pt NP/block copolymer hybrid materials with varying morphologies.

Experimental Section

Materials and Instrumentation. *Materials*. For the block copolymer synthesis, *sec*-butyllithium (1.4 M in cyclohexane, Aldrich) was used as received. Isoprene (99%, Aldrich), cyclohexane (99%, J. T. Baker), tetrahydrofuran (THF) (99%, J. T. Baker), and 1, 1-diphenylethylene (97%, Aldrich) were distilled from *n*-butyllithium (1.6 M in hexanes, Sigma-Aldrich) prior to use. 2-(Dimethylamino)ethyl methacrylate (DMAEMA) (98%, Aldrich) was stirred over CaH_2 (90%-95%, Aldrich) overnight and distilled under vacuum. Methanolic HCl (3 N, Supelco) was degassed with a freeze−pump−thaw process three times prior to use.

For the ligand synthesis, 2-allyloxyethanol (Aldrich, 98%) was stirred over CaH_2 overnight and distilled under vacuum prior to use. 1,3-Dibromopropane (Sigma-Aldrich, 99%) was distilled under vacuum prior to use. Pyridine (Aldrich, anhydrous 99.8%), phosphorus tribromide (Aldrich, 98%), 33 wt % methylamine in ethanol (Aldrich), sodium carbonate (Sigma-Aldrich, 98%), methanol (J. T. Baker, anhydrous), methanol (Aldrich, anhydrous, 99.8%), sodium hydrosulfide hydrate (Aldrich), 35 wt % hydrochloric acid aqueous solution (Sigma-Aldrich), potassium hydroxide (Sigma-Aldrich, 97%), chloroform (J. T. Baker, 99%), and magnesium sulfate (Sigma-Aldrich, anhydrous, 99%) were used as received.

For the nanoparticle synthesis and hybrid synthesis, platinum(IV) chloride (Aldrich, 99.9%), sodium borohydride (Sigma-Aldrich, 99%), methanol (J. T. Baker, anhydrous), ethyl ether (J. T. Baker, anhydrous), and chloroform (J. T. Baker, 99%) were used as received.

Instrumentation. ^{1}H solution nuclear magnetic resonance (^{1}H NMR) spectra were recorded on a Varian INOVA 400 MHz spectrometer using $CDCl_3$ signal (δ = 7.27 ppm) as an internal standard. Small angle X-ray scattering (SAXS) data were obtained on a home-built Rigaku RU3HR Cu Kα rotating anode beamline. Detailed instrumental setup is described elsewhere.[35] For transmission electron microscopy (TEM), hybrid samples were sectioned with a Leica Ultracut UCT cryo-ultramicrotome at −60 °C. Sample slices were collected on a water/dimethyl sulfoxide 60%/40% (v/v) solution surface and transferred to copper TEM grids. Pt NP TEM samples were prepared by dissolving the NPs in methanol, ultrasonicating the solution for 1 min, and dropping 5 μL of the solution to a carbon-supported copper TEM grid with a pipet. Bright field (BF-TEM) images were taken with a FEI Tecnai T12 Spirit electron microscope equipped with a SIS Megaview III CCD camera, operated at an acceleration voltage of 120 kV. High angular annular dark field scanning transmission electron microscopy (HAADF-STEM) images were taken with a FEI Tecnai F20 field emission electron microscope at an acceleration voltage of 200 kV. Thermogravimetric analysis (TGA) was performed using a TA Instruments Q500 instrument equipped with an autosampler. Measurements were taken by heating from 20 to 550 °C at 10 °C/min.

Material Synthesis. PI-*b*-PDMAEMA block copolymers were synthesized using anionic polymerization according to a method described elsewhere.[38] The ligand and Pt NP syntheses as well as NP aging were performed as described in reference 35.

Pt NP size was characterized by BF-TEM and HAADF-STEM. The composition of ligand-coated Pt NPs was characterized by TGA under flowing nitrogen. The mass fraction of ligands which was converted into residual carbon after pyrolysis in nitrogen environment was assumed to be consistent (26%) to that obtained previously.[35]

Both the aged NPs and as-made NPs were found to irreversibly aggregate in methanol after extended storage in air (1 month), which could be due to the desorption (oxidation) of the ligands. Thus, all nanoparticles were used within 2 weeks after their synthesis.

Hybrid Synthesis. Mixtures of aged ligand-stabilized Pt NPs and PI-*b*-PDMAEMA were dissolved in 10 wt % methanol/chloroform 1:9 (w/w) solutions and stirred for at least 1 h. The solutions were cast on 1 cm diameter aluminum Petri dishes on a hot plate at 50 °C. During casting, a glass hemisphere was used to cover the hot plate and a crystallization dish (diameter 6 cm) full of chloroform was used to slow down chloroform evaporation from the methanol-chloroform mixture. The as-made films were further annealed in a vacuum oven at 110 or 130 °C for at least 2 days.

Hybrid Disassembly. Hybrid samples were disassembled by putting small pieces into cyclohexane or THF (~0.1% w/w) and stirring the solution for 4 h. For TEM investigation a drop of the resulting solution was put on a TEM copper grid and dried before imaging.

Results and Discussion

1. Nanoparticle Ligand Density. The platinum nanoparticles in this work were synthesized via one-phase reduction of metal salts in the excess environment of thiol ligand molecules, followed by the removal of excess ligand and salt.[35] After synthesis, the nanoparticles were "aged" by refluxing in water to remove some of the ligands and then were thoroughly washed. In our previous report, based on bright field transmission electron microscopy (BF-TEM) results, the number of thiol ligand molecules on one Pt NP was calculated to be 92 and 65 before and after the aging process, respectively, which corresponds to an area occupied by one thiol headgroup of 0.111 and 0.157 nm^2, respectively.[35] In this section, we will revisit the question of the ligand density on the Pt NPs, this time based on particle size distribution data obtained from high-angle annular dark field scanning transmission electron microscopy (HAADF-STEM) image analysis.

In the work of Warren et al., we calculated the number of ligands for a Pt NP under the following assumptions:[35]

1. All Pt NPs are assumed to have an average diameter d = 1.83 nm.
2. Pt NPs are spherical and have the same density as bulk platinum metal.
3. The average weight fraction of ligands on the Pt NPs can be derived from the TGA mass loss.

(38) Creutz, S.; Teyssie, P.; Jerome, R. *Macromolecules* **1997**, *30*, 5596.

4. The ligand molecular weight after particle synthesis is identical to that of the originally synthesized ligand, with the same counterion ratio between bromides and chlorides.
5. All ligand that is present is bound directly to the nanoparticle surface, which is supported by NMR analysis.[35]

Here, we want to take a closer look at the first assumption. As the metal particle size decreases, the surface area to volume ratio (S/V) increases, which leads to a higher ligand content per unit mass of Pt for smaller NPs. Rather than using average values for the radius, a more accurate assumption is to linearly correlate the surface area of Pt NPs to the number of ligands. In order to obtain the surface area of Pt NPs, one needs to determine the accurate particle size distribution including subnanometer NPs, which is difficult to obtain from BF-TEM due to the lack of contrast.[39] HAADF-STEM imaging is a more effective technique for this problem since it collects electrons scattered at larger angles (>5°) and, therefore, provides high contrast images for large atomic number species.[40]

Figure 2 shows the HAADF-STEM images of the Pt NPs from batches that were used to form nanostructures with block copolymers. The histograms derived from these images revealed the following:

1. A large number of subnanometer NPs are distinctly visible in HAADF-STEM images, while the bright field TEM images do not provide enough contrast to show such small particles. The formation of metal nanoclusters (i.e., nanoparticles smaller than 1 nm)[41,42] in the presence of thiols have been reported for other metals such as silver, gold, and palladium.[43−45]
2. Compared to as-made NPs (top left in Figure 2), aged NPs (top right in Figure 2) have a broader size distribution toward larger particles. We note, however, that the subnanometer particles are still present in significant quantities even after the aging process.

Calculation of the thiol head area density from this new HAADF-STEM data yielded 0.173 nm^2 per thiol group (see the Supporting Information for details). The aged NPs yielded 0.196 nm^2 per thiol following the same calculation. For comparison, the area per thiol headgroup for a methanethiol-coated Pt{111} surface is 0.200 nm^2.[46] Many factors affect the area per thiol headgroup on metal surfaces, including surface curvature, existence of metal nanocrystal defects such as edges, steps, and vertices, and tail size of the ligand.[39,47−51] The fact that the NP ligand density is similar to that of a simple alkanethiol on a flat Pt surface suggests that the effects from the high NP surface curvature cancels the steric effect from the large tail volume, allowing a large conical angle for the ligand molecule rotation.

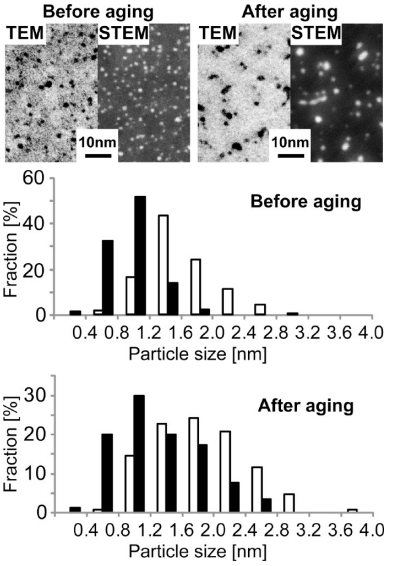

Figure 2. (top) BF-TEM and HAADF-STEM images of Pt NPs before and after aging process. (middle/bottom) Histograms of Pt NP size distributions obtained from BF-TEM and HAADF-STEM images. White bars refer to the distribution from BF-TEM images, and black bars refer to that from HAADF-STEM images.

2. Hybrid Morphology Exploration. We investigated PI-*b*-PDMAEMA/Pt NP self-assembly with two different PI-*b*-PDMAEMA block copolymers, referred to as MK31 (31 000 g/mol, 33 wt % PDMAEMA) and MK29 (29 000 g/mol, 17 wt % PDMAEMA). The polydispersity index (PDI) of both polymers was below 1.1 (M_w/M_n = 1.03 and 1.06, for MK31 and MK29, respectively, where M_w is weight average molecular weight and M_n is number average molecular weight).

We prepared a series of hybrid samples by varying Pt NPs/PI-*b*-PDMAEMA ratios. All the Pt NPs used to synthesize hybrids were aged, with ligand headgroup densities of ~0.196 nm^2 per thiol, following the calculation discussed above. Table 1 lists the Pt NPs/PI-*b*-PDMAEMA ratios of

(39) Eklund, S. E.; Cliffel, D. E. *Langmuir* **2004**, *20*, 6012.
(40) Otten, M. T. *J. Electron Microscopy Technique* **1991**, *17*(2), 221–230.
(41) The terms *nanoparticle*, and *nanocluster* are loosely defined. According to literature,[42] the term nanoparticle refers either "to all 0 D nanosized building blocks" or "amorphous or semicrystalline 0 D nanostructures with dimensions larger than 10 nm." Nanoclusters, on the other hand, refer to smaller-sized nanostructures. In this article we use the term nanoparticles for our platinum nanomaterials to maintain consistency with our previous publications.[35,36]
(42) Fahlman, B. D. *Materials Chemistry*; Springer: Dordrecht, The Netherlands, 2007.
(43) Dance, I. G.; Fisher, K. J.; Banda, R. M. H.; Scudder, M. L. *Inorg. Chem.* **1991**, *30*, 183.
(44) Jadzinsky, P. D.; Calero, G.; Ackerson, C. J.; Bushnell, D. A.; Kornberg, R. D. *Science* **2007**, *318*, 430.
(45) Zamborini, F. P.; Gross, S. M.; Murray, R. W. *Langmuir* **2001**, *17*, 481.
(46) Kim, S. S.; Kim, Y.; Kim, H. I.; Lee, S. H.; Lee, T. R.; Perry, S. S.; Rabalais, J. W. *J. Chem. Phys.* **1998**, *109*, 9574.
(47) Love, J. C.; Estroff, L. A.; Kriebel, J. K.; Nuzzo, R. G.; Whitesides, G. M. *Chem. Rev.* **2005**, *105*, 1103.
(48) Hostetler, M. J.; Stokes, J. J.; Murray, R. W. *Langmuir* **1996**, *12*, 3604.
(49) Hostetler, M. J.; Wingate, J. E.; Zhong, C.-J.; Harris, J. E.; Vachet, R. W.; Clark, M. R.; Londono, J. D.; Green, S. J.; Stokes, J. J.; Wignall, G. D.; Glish, G. L.; Porter, M. D.; Evans, N. D.; Murray, R. W. *Langmuir* **1998**, *14*(1), 17–30.
(50) Luedtke, W. D.; Landman, U. *J. Phys. Chem. B* **1998**, *102*(34), 6566–6572.
(51) Hill, H. D.; Millstone, J. E.; Banholzer, M. J.; Mirkin, C. A. *ACS Nano* **2009**, *3*, 418.

Table 1. Summary of Hybrids' Hydrophilic Volume Fraction and Corresponding Morphology

sample	PI-*b*-PDMAEMA M_n (kg/mol)	PDMAEMA fraction (wt %)	Pt NPs/PI-*b*-PDMAEMA weight ratio	hydrophilic domain volume ratio[a]	morphology	q^* (1/nm)
MK29-1	29	17	0.52	0.25	spherical	0.28
MK29-2	29	17	0.76	0.29	spherical	0.26
MK29-3	29	17	1.0	0.33	wormlike micelle	0.23
MK29-4	29	17	1.54	0.41	wormlike micelle	0.18
CCM-Pt-4[c]	31	33	2.2	0.55	lamellae	0.19
MK31-1[b]	31	33	(3.5)	(0.65)	lamellae	0.17
MK31-2	31	33	3.0	0.62	lamellae + inverse hexagonal	0.18
MK31-3	31	33	3.2	0.63	inverse hexagonal	0.21
CCM-Pt-6[c]	31	33	3.5	0.65	inverse hexagonal	0.21

[a] Hydrophilic domain volume ratio (Pt NPs/PI-*b*-PDMAEMA volume ratio) were calculated according to ρ(PI) = 0.91 g/mol, ρ(PDMAEMA) = 1.15 g/cm^3, ρ(Pt) = 21.09 g/cm^3, ρ(ligand) = 1.3 g/cm^3. [b] Sample showed precipitation of particles. [c] Sample shown in a previous report.[35]

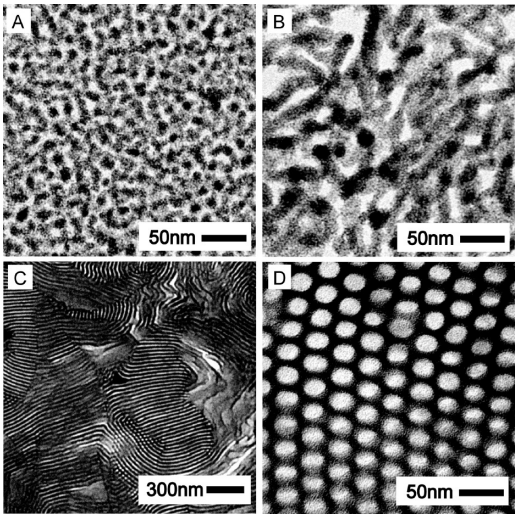

Figure 3. Representative bright field TEM images: (A) spherical micellar morphology (MK29-2); (B) wormlike cylinders morphology (MK29-3); (C) lamellar morphology (MK31-1); (D) inverse hexagonal morphology (MK31-3).

different hybrids and the corresponding morphologies obtained, as suggested by a combination of small-angle X-ray scattering and TEM analysis, see below. The table also includes the results of our previous report.[35] As the volume fraction of the inorganic content increases, four different morphologies were obtained as revealed by BF-TEM (see Figure 3): spherical micelles (Figure 3A), wormlike micelles (Figure 3B), lamellae (Figure 3C), and inverse hexagonal cylinders (Figure 3D). In the BF-TEM images, PI appears as bright domains while PDMAEMA/Pt NPs appear dark, with contrast arising from the electron density difference between the different domains. We note that when more NPs were added to MK29 with the shorter PDMAEMA chains (5000 g/mol for MK29 versus 10 000 g/mol for MK31), macrophase separation with aggregated NPs was observed. Also, in some of the films that used MK29, occasionally NP agglomeration was observed along with microphase separated structures. All these observations suggest that MK29's PDMAEMA chains may be at the lower limit relative to the NP size necessary to observe good structure control. The radius of gyration calculated

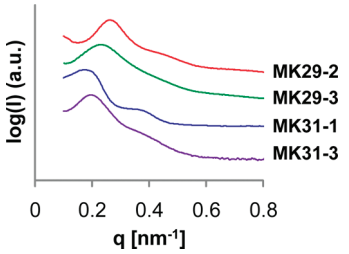

Figure 4. Small angle X-ray scattering (SAXS) patterns from annealed BCP/Pt NP hybrids. The curves show the intensity profiles for spherical micellar, wormlike micellar, lamellar, and inverse hexagonal morphologies, from top to bottom.

for MK31 and MK29 are 2.5 and 1.8 nm, respectively.[52] Indeed, the radius of gyration of MK29 is very close to the average Pt NP size, inconsistent with criterion no. 3 in the introduction that the NP size should be smaller than the radius of gyration of the mixing block.

Figure 4 shows the small-angle X-ray scattering (SAXS) patterns of annealed hybrids with the four different morphologies. Although the patterns display too few orders to unambiguously determine phases, if one assumes phases indicated by TEM (Figure 3), the position of the first order is a consistency check of the structure. Here, the scattering vector q is defined as $q = 4\pi \sin\theta/\lambda$, where 2θ is the scattering angle and λ is the wavelength of the Cu Kα X-ray beam, 1.54 Å. The term q^* signifies the position of the first peak in the scattering pattern. The first Bragg reflection for the lamellar hybrid MK31-1 at 0.17 nm^{-1} corresponds to an interplanar spacing of 36 nm, while that for the inverse hexagonal hybrid MK31-3 at 0.21 nm^{-1} corresponds to an channel-to-channel spacing ((10) period in the hexagonal lattice) of 35 nm. Both spacings are consistent with the periods of the nanostructures measured from BF-TEM images. We note that in most hybrids, due to the small grain size of the nanostructures (generally smaller than a couple of micrometers, corresponding to 40−50 repeat units at most in thermally annealed films) coupled with the large X-ray attenuation from Pt, higher-order reflections were not clearly distinguished.

From both SAXS and TEM data of samples with lower NP loadings, the morphologies obtained had particularly limited long-range orders. It has to be noted that thin sections of samples for TEM (Figure 3A and B) were

(52) Santore, M. M.; Kozlova, N. Nanopatterned Surfaces and Related Methods for Selective Adhesion, Sensing and Separation. U. S. Patent Application, 11/592,454, **2006**.

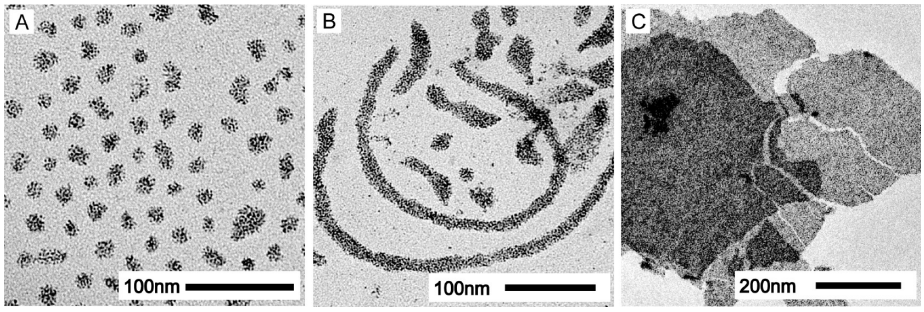

Figure 5. Representative bright field TEM images of isolated nano-objects: (A) spheres from sample MK29-2; (B) wormlike cylinders from sample MK29-4; (C) lamellar sheets from sample MK31-1. Contrast variations in C suggest single sheets (right side), overlapping sheets (left side), and even higher-order aggregates (upper left corner).

sliced using cryo-ultramicrotoming at the water/DMSO eutectic temperature of −60 °C, which is around the glass transition temperature (T_g) of PI (−60 °C). Thus, structure deformation during (or after) microtoming cannot be excluded and is rather very likely for samples with PI majority phase. When Pt NPs/PDMAEMA domains make up the majority part of the hybrids, however, low T_g PI domains are embedded within a higher T_g framework (T_g of PDMAEMA ~ 20 °C). No distortions are thus expected during the sample preparation process, consistent with our observations in TEM (Figure 3C and D).

3. Isolated Nano-objects Disassembled from Hybrids. We have shown that hybrids with inverse hexagonal morphology can be subsequently pyrolyzed followed by acid or plasma treatment to remove the block copolymer, generating a nanoporous metal 3D framework.[35] In contrast, similar heat treatments of hybrids without interconnected inorganic network structures such as lamellar and micellar films will lead to a collapse of the 3D structure. For poly(isoprene-*block*-ethylene oxide) (PI-*b*-PEO)/aluminosilicate hybrid films with a dispersed inorganic phase, Ulrich et al. showed that isolated polymer−ceramic hybrid nano-objects with well-defined shape and size consist with inorganic/PEO cores and PI shells can be achieved through dissolution in organic solvents.[53] For the PI-*b*-PDMAEMA/Pt NPs system, we thus explored the formation of shape and size controlled metallic nano-objects with Pt/PDMAEMA cores and PI shells from disassembly experiments.[34,54−56] Indeed, by stirring hybrid films with spherical, wormlike micellar, and lamellar morphologies in cyclohexane or tetrahydrofuran for 4 h, isolated spheres, cylinders and nanosheets were obtained, respectively, as shown in Figure 5. Figure 5A shows nanospheres obtained from micellar structures. Dissolution of wormlike micelles leads to isolated cylinders with different aspect ratios, see Figure 5B. Nanosheets were obtained from dissolution of lamellar hybrids, see Figure 5C. It should be noted that these results provide independent proof of the structure assignments that were based on SAXS and TEM results in the previous section. In analogy to what was observed for the PI-*b*-PEO/aluminosilicate system, the current nano-objects have a core−shell structure with a PDMAEMA/Pt NP core and PI chains as a shell, increasing the solubility and providing colloidal stability of the nano-object in organic solvents.[53] Since PI chains provide only low contrast, the TEM images only show the core of the nano-objects. High resolution images of these isolated nanostructures further confirm that the cores consist of small Pt NPs (data not shown, as is already evident from Figure 5).

The average size of the spheres obtained by dissolution of samples MK29-1 and MK29-2 increased from 14 to 17 nm, respectively, consistent with increasing Pt NP/BC ratios of the hybrids. Likewise, the average dimensions of the nanocylinders disassembled from hybrids MK29-3 and MK29-4 increased from 12 to 16 nm. The length of the cylinders as well as the size of the nanosheets obtained from lamellar hybrids was not very well-defined, ranging from several hundred nanometers to several micrometers. As demonstrated before for aluminosilicate cylinders, the length (size) of the nano-objects can be tailored, for example, through ultrasonication, making this a powerful tool for the formation of well-defined nano-objects.[6,57] These nano-objects are stable in solution for at least one week both in cyclohexane and in THF (data not shown), indicating that the NPs and PDMAEMA formed an integrated composite.

Conclusion

We have successfully formed BCP/metal hybrid materials from functional ligand-stabilized Pt NPs and amphiphilic PI-*b*-PDMAEMA diblock copolymers, with increasing metal loadings leading to four distinct nanocomposites. The ligand functionality containing an ionic part and a hydrophilic tail with steric hindrance ensures high NP solubility in polar solvents as well as compatibility with the hydrophilic block of the BCP. The Pt NP size distribution was measured by HAADF-STEM, which enabled a more accurate estimate of the ligand headgroup density of the Pt NPs. Disassembly of hybrids without a continuous inorganic phase resulted in metallic nano-objects with core−shell architecture and

(53) Ulrich, R.; Du Chesne, A.; Templin, M.; Wiesner, U. *Adv. Mater.* **1999**, *11*, 141.
(54) Li, F.; Wang, Z.; Stein, A. *Angew. Chem., Int. Ed.* **2007**, *46*, 1885.
(55) Li, F.; Delo, S. A.; Stein, A. *Angew. Chem., Int. Ed.* **2007**, *46*, 6666.
(56) Lin, X.; Wang, Y.; Wu, L. *Langmuir* **2009**, *25*, 6081.
(57) Wang, X.; Guerin, G.; Wang, H.; Wang, Y.; Manners, I.; Winnik, M. A. *Science* **2007**, *317*, 644.

well-defined shapes. By further tuning of metal NP/BCP hybrid systems through block copolymer structure/chemistry variations and/or nanoparticle compositions, other morphologies such as bi- or triply continuous structures particularly interesting for energy related applications[3,58] as well as mixed metals based ordered nanostructures should become accessible which may exhibit novel optical, magnetic, or catalytic properties.

Acknowledgment. This publication was supported by a subcontract with Cornell University, Department of Materials Science and Engineering, under Prime Agreement Award Number 06-G-031 from the Department of Homeland Security, by Grant Number R21DE018335 from the National Institute of Dental and Craniofacial Research, by the U.S. Department of Energy (Grants DE-FG02-03ER46072 and DE-FG02-97ER62443), and by NSF DMR-0605856 and DMR-0404195. Research made use of facilities of the Cornell Center for Materials Research (CCMR) with funding from the Materials Research Science and Engineering Center program of NSF (cooperative agreement DMR-0520404). We thank Prof. Francesco Stellacci in the Department of Materials Science and Engineering, Massachusetts Institute of Technology, and Dr. Osman Bakr in the School of Engineering and Applied Science, Harvard University, for pointing out the ligand density issue with the Pt NPs, and fruitful discussions about the formation of metal nanoclusters. The content of this publication is solely the responsibility of the authors and does not necessarily represent the official view of any of the funding agencies.

Supporting Information Available: Calculation of the thiol headgroup area from HAADF-STEM data. This material is available free of charge via the Internet at http://pubs.acs.org.

(58) Crossland, E. J. W.; Kamperman, M.; Nedelcu, M.; Ducati, C.; Wiesner, U.; Smilgies, D. F.; Toombes, G. E. S.; Hillmyer, M. A.; Ludwigs, S.; Steiner, U.; Snaith, H. J. *Nano Lett*. **2009**, *9*, 2807.

Supporting Information

Metal Nanoparticle/Block Copolymer Composite Assembly and Disassembly

Zihui Li,[†,‡] *Hiroaki Sai,*[†,§] *Scott C. Warren,*[‡] *Marleen Kamperman,*[§] *Hitesh Arora,*[‖] *Sol M. Gruner,*[#,▽] *and Ulrich Wiesner*[*,§]

[‡]Department of Chemistry and Chemical Biology, Cornell University, Ithaca, NY, 14853

[§]Department of Materials Science and Engineering, Cornell University, Ithaca, NY, 14853

[‖]Department of Chemical and Biomolecular Engineering, Cornell University, Ithaca, NY, 14853

[#]Department of Physics, Cornell University, Ithaca, NY, 14853

[▽]Cornell High Energy Synchrotron Source (CHESS), Cornell University, Ithaca, NY, 14853

[†] These authors contributed equally to this work.

[*] To whom correspondence should be addressed. Email Address: ubw1@cornell.edu

The following discussion contains the calculation of the thiol head group area from the Pt NP size distribution from HAADF-STEM images. From TGA analysis (data not shown), the as-made NPs, on average, contained 55.5 wt. % Pt, and the aged NPs contained 64.2 wt. % Pt. The following equations refer to the as-made NPs.

The total Pt mass for the ensemble of 118 NPs in a TEM image (a portion of the image is available in Figure 2) is estimated from the nanoparticle size distribution shown in the middle row of Figure 2 in the main text and the bulk density of the platinum metal, $\rho = 21.45$ g/cm^3:

$$M_{Pt} = \rho \cdot \sum \frac{4}{3}\pi r^3 = 1.749 \cdot 10^{-18}\,\mathrm{g} \qquad [1]$$

where r is the radius of each particle core and the summation is over all particles of the measured size distribution. The total surface area, S, for this ensemble is:

$$S = \sum 4\pi r^2 = 4.410 \cdot 10^{-16}\,\mathrm{m}^2 = 441.0\,\mathrm{nm}^2 . \qquad [2]$$

Therefore the area that one thiol occupies on the platinum surface is:

$$\frac{S}{\#\,\text{of ligands}} = 441.0\mathrm{nm}^2 \Big/ \left[\frac{\left(\frac{1.749 \cdot 10^{-18}\,\mathrm{g}}{0.555} \right) - 1.749 \cdot 10^{-18}\,\mathrm{g}}{331.7\ \mathrm{g/mol}} \cdot \frac{6.022 \cdot 10^{23}\,\text{ligands}}{\mathrm{mol}} \right] = 0.173\,\mathrm{nm}^2/\text{ligand} . \qquad [3]$$

Here 331.7 g/mol is the molar mass of the ligand in Figure 1A in the main text.[1]

REFERENCES

(1) Warren, S. C.; Messina, L. C.; Slaughter, L. S.; Kamperman, M.; Zhou, Q.; Gruner, S. M.; DiSalvo, F. J.; Wiesner, U. *Science* **2008,** *320*, 1748.